THE JOURNAL OF PHYSICAL CHEMISTRY B

Article

pubs.acs.org/JPCB

Probing the Contribution of Different Intermolecular Forces to the Adsorption of Spheroproteins onto Hydrophilic Surfaces

João Borges,* José M. Campiña,* and A. Fernando Silva

Centro de Investigação em Química-Linha 4 (CIQ-L4), Departamento de Química e Bioquímica, Faculdade de Ciências, Universidade do Porto, Rua do Campo Alegre, 687, 4169-007, Porto, Portugal

Supporting Information

ABSTRACT: Protein adsorption is a delicate process, which results from the balance between the properties of proteins and their solid supports. Although the relevance of some of these parameters has been already unveiled, the precise involvement of electrostatics and other weaker intermolecular forces requires further comprehension. Aiming to contribute to this task, this work explores the attachment, rearrangement, and surface aggregation of a model spheroprotein, such as bovine β-lactoglobulin (β-LG), onto hydrophilic substrates prefunctionalized with different alkylthiol films. Thereby, a variety of electrostatic scenarios for the adsorption of β-LG could be recreated through the variation of the pH and the functional chemistry of the surfaces. The changes in surface mass density (plus associated water) and film flexibility were followed in situ with quartz crystal microbalance with dissipation monitoring. Film packing and aggregation were assessed by faradaic electrochemical measurements and ex situ atomic force microscopy and field effect scanning electron microscopy. In contrast to previous hypotheses arguing that electrostatic interactions between charged substrates and proteins would be the only driving force, a complex interplay between Coulombic and non-Coulombic intermolecular forces (which would depend upon the experimental conditions) has been suggested to explain the results.

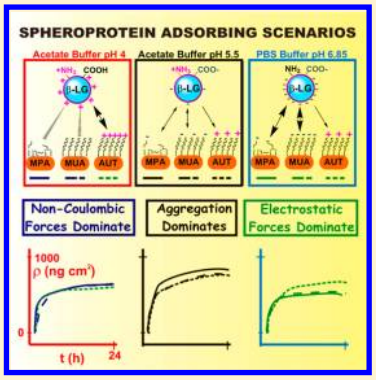

1. INTRODUCTION

Almost one decade ago, Nakanishi and co-workers defined the adsorption of proteins onto solid surfaces as a "common" but "complicated" phenomenon.[1] The first of these claims is well exemplified by its wide involvement in a variety of fields such as medicine, analytical and pharmaceutical sciences, biotechnology, cell biology, and the food industry.[2] A better understanding of protein adsorption onto hard/soft matter is fundamental in advancing our knowledge on cellular processes, the principles guiding the engineering of protein-resistant materials, and the properties of nanomaterials in physiological environments.[3,4] With an impending revolution in the medical field triggered by the incorporation of emerging nanotechnologies, it seems a not too risky prophesy that the full comprehension and control of interfacial protein adsorption is one of the top challenges to be addressed by novel nanobiotechnologies.[3,5]

The characteristics of a given surface and protein; which can be influenced by external parameters such as the temperature (affecting the kinetics of the process),[6,7] the pH (which determines the charge density at proteins and surfaces),[8,9] or the ionic strength (which regulates the damping distance of the electric field created by charged proteins and, consequently, the intensity of the Coulombic forces established between them),[10] are well-known to have an important weight in these processes.[11] In this sense, the size, shape, structure, and isoelectric point of proteins are some of the relevant parameters. For instance, small and relatively hard proteins, such as β-lactoglobulin (β-LG) or lysozyme, diffuse much faster than immunoglobulins or fibrinogens, which are larger and softer. It is well-known that the latter bind more strongly to surfaces and that they can even repel preadsorbed proteins during postadsorption spreading because of an enhanced contact area.[12] Although both can relax to a certain extent onto hydrophobic surfaces via interaction with the hydrophobic cores, the lower internal stability of "soft" proteins makes them more prone to suffer a significant loss of tertiary structure.

That is the complicated part referred to by Nakanishi; that is, there are many parameters with the potential to affect the folding/unfolding phenomena followed by proteins after their attachment to a surface. Moreover, these processes are characterized out of equilibrium most of the times due to a very slow kinetics. Despite these limitations, a great influence has been already demonstrated for surface properties such as topology, roughness, polarity, and energy.[8,13−15] Regarding the electrostatic adsorption of proteins, beyond a couple of theoretical contributions of Lenhoff and co-workers in the mid 1990s,[16,17] it has been typically described as governed by the net protein charge.[18−21] On the contrary, an increasing body of theoretical and experimental evidence is pointing toward significant adsorption of charged proteins onto noncharged surfaces and vice versa.[22−25] These observations

Received: September 16, 2013
Revised: December 2, 2013
Published: December 5, 2013

dx.doi.org/10.1021/jp409238b | J. Phys. Chem. B 2013, 117, 16565−16576

undoubtedly indicate that, due to the structural complexity of proteins, they must undergo a variety of forces beyond the purely electrostatic ones. In line with this view, Kasemo et al. stated very recently that the correlation between net charge and adsorption behavior is a simplistic "approximation that needs a further deeper investigation".[26]

Because proteins can be immobilized in a wide range of surfaces, the chosen one must reflect the scientific context of the work. To this end, the self-assembled monolayers (SAMs) formed by alkylthiols ($C_nH_{2n+1}SX$) on Au surfaces (which produce relatively dense, well-ordered, and chemically stable 2D films)[27−29] seem more suitable than polymers,[18,30] polyelectrolytes,[20,31] electrodeposited solid layers,[30] and lipid membranes[19,26,32−35] as model platforms to investigate the role of different intermolecular forces in the particularities of protein adsorption. Through such an approach, more limited contributions from the viscoelasticity and roughness of the substrate (an element of uncertainty, for instance, when lipid membranes are used) are expected. Furthermore, by selecting the functional end group of the given thiol (X), its chain length (n), and the appropriate experimental conditions, one can tune the chemical composition, structure, and charge of these substrates.

In this Article, we aim to get deeper insights on the involvement of different intermolecular forces in the adsorption of a "hard" globular protein (or spheroprotein), such as bovine β-LG (the main protein in cow milk[36] and a typical model in studies on milk's surface tension[37] and protein adsorption[38,39]). To this end, β-LG was adsorbed from solutions buffered at three different pH's onto hydrophilic substrates coated with SAMs of three different alkylthiols. Thereby, different electrostatic scenarios could be recreated through the simple selection of alkylthiol and pH. The changes in mass and energy dissipated by the adsorbed films were followed in a time-resolved mode by means of the quartz crystal microbalance with energy dissipation monitoring (QCM-D). Atomic force microscopy (AFM) and field effect scanning electron microscopy (FESEM) were applied ex situ to inspect the distribution of adsorbed proteins with special regard to aggregation issues. To complete the study, the electrochemical behavior of the films was investigated through cyclic voltammetry (CV) and electrochemical impedance spectroscopy (EIS) in the presence of $[Fe(CN)_6]^{3-/4-}$ probes.

2. EXPERIMENTAL SECTION

2.1. Materials. Bovine β-lactoglobulin (PSDI-2400, 95%, variants A+B) was supplied by Arla Foods Ingredients (Videbaek, Denmark). A complete characterization of this reagent can be found elsewhere.[21] 11-Amino-1-undecanethiol hydrochloride (>90%, AUT) was purchased from Dojindo Laboratories. 3-Mercaptopropionic acid (>99%, MPA) and 11-mercapto-1-undecanoic acid (98%, MUA) were acquired from Sigma-Aldrich. Other chemicals, glacial acetic acid (Merck, >99%, CH_3COOH), sodium acetate (Sigma-Aldrich, 99%, CH_3COONa), monopotassium and dipotassium phosphate (Sigma-Aldrich, KH_2PO_4 and K_2HPO_4), tetrapotassium hexacyanoferrate trihydrate (Fluka, >98.5%, $K_4[Fe(CN)_6]\cdot 3H_2O$), and tripotassium hexacyanoferrate (Fluka, 99%, $K_3[Fe(CN)_6]$), were all analytical grade and used without further purification. Stock solutions of 50 mM acetate buffer (ACB, pH 4 and 5.5) and 50 mM phosphate buffer (PB, pH 6.85) were prepared using ultrapure water from a Milli-RO 3 Plus coupled with a Milli-Q water purification system (18.2 MΩ cm resistivity).

2.2. Methods. Adsorption processes were followed in situ at 25 °C using a QCM-Z500 multifrequency quartz crystal microbalance with impedance and dissipation energy monitoring from KSV Instruments (Finland). Further details on the technique and the instrument can be found elsewhere.[31,40] 5 MHz overtone polished AT-cut plano−plano quartz crystal plates coated with gold electrodes (surface area S = 0.785 cm^2, KSV Instruments, since now the plates) were used for QCM-D measurements. The results herein presented correspond to the shifts in dissipation factor and normalized frequency gathered at the fifth overtone (25 MHz), ΔD_5 and $\Delta f_5/5$, respectively, as they presented the lowest levels of noise. Frequency shifts were converted into mass uptakes ($\rho = \Delta m/S$, with Δm being the mass shifts) by means of Sauerbrey's equation ($\Delta f_5/5 = -C_f\rho$; the sensitivity factor for these plates is C_f = 55.5 Hz μg^{-1} cm^2). Sauerbrey's model assumes that the loaded mass is evenly distributed in a rigid film, which dissipates negligible energy in its oscillation (for more details, see the Supporting Information). Thereby, the values of ρ (the mass deposited per unit area) must necessarily contain contributions from trapped water even in the case of the most rigid protein layers.[41]

A double exponential equation derived from the random sequential adsorption (RSA) theory was used to model the adsorption kinetics[15] (see the Supporting Information for more details):

$$\rho = (1/A_1)(\exp[2.3A_1k_1Ct] - 1) + (1/A_2)(\exp[2.3A_2k_2Ct] - 1) \quad (1)$$

While the first exponential describes the kinetics at short times (when proteins initially approach to a barely covered surface), the second represents the behavior at longer times when the coverage is much higher and adsorbed proteins can undergo structural rearrangements. Whether the rate constants (k) are given in cm min^{-1}, the bulk concentration of β-LG (C) in ng cm^{-3}, and the adsorption time (t) in min (the steric factors, A, are nondimensional constants that represent the steric hindrance felt by proteins on their way to the surface), ρ is given in ng cm^{-2}.

A PicoLe 5100 atomic force microscope (Agilent Technologies, U.S.) was operated in tapping mode over 5 × 5 μm^2 regions of the plates after proper drying under a soft stream of N_2. Topography, amplitude, and phase images were taken in air, with a resolution of 512 × 512 pixels, using silicon cantilevers (ACT-50, AppNano, U.S.) with a pyramidal-shaped tip (spring constant, 25−75 N/m; resonance frequency, 200−400 kHz). Raw AFM data were corrected for bow/tilt using the software PicoViewTM 1.8.2 and further analyzed using the freeware Gwyddion 2.25. Statistical data were extracted from three different images and averaged for each single sample (with the standard deviation being taken as the corresponding error). FESEM experiments in the secondary, and backscattered, electron modes (working distance, 8.5−10.8 mm; accelerating voltage, 10−20 kV) were performed in a FEI Quanta 400 FEG scanning electron microscope (CEMUP, Centro de Materiais da Universidade do Porto).

The wettability of the functionalized plates was determined in air through the static sessile drop method in a contact-angle goniometer. Ultrapure water was used as liquid phase (5 μL drops). The measurements were repeated three times and averaged for each surface. Faradaic CV and EIS experiments were performed in triplicate at 25 °C using an AUTOLAB

Table 1. Physicochemical Properties of the Different Alkylthiols Used in This Work and Contact Angle Data (θ) Measured for the Corresponding Au/SAM Surfaces

alkylthiol	n	X	formula	M_W/g mol^{-1}	pK_a	θ^d/deg
MPA	2	−COOH	$C_3H_6SO_2$	106.14	5.2 ± 0.1[a]	44 ± 1
MUA	10	−COOH	$C_{11}H_{22}SO_2$	218.36	5.7 ± 0.2[b]	56 ± 1
AUT	11	−NH_2	$C_{11}H_{25}NS$	239.85	7.5 ± 0.5[c]	57 ± 1

[a]According to ref 42. [b]Reference 43. [c]Derived from ref 44. [d]$\theta_{\text{bare Au}}$ = 77 deg.

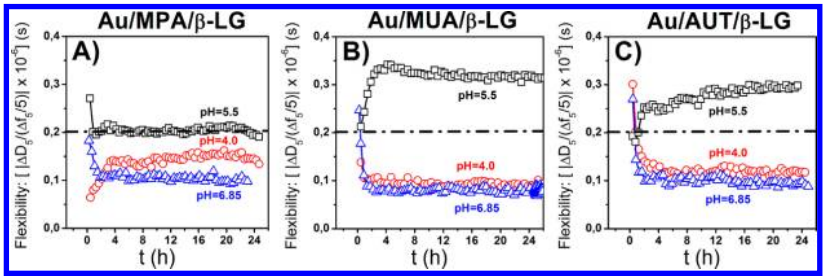

Figure 1. Variations in the flexibility factor (given as the absolute value of the ratio between the dissipation factor and the normalized frequency shifts at the fifth overtone: $|\Delta D_5/(\Delta f_5/5)|$) that occurred at Au/MPA (A), Au/MUA (B), and Au/AUT quartz plates (C), for 24 h after the injection of a 50 μg mL^{-1} β-LG solution in 50 mM ACB pH 5.5 (□), 50 mM ACB pH 4.0 (red ○), and 50 mM PB at pH 6.85 (blue △).

PGSTAT 302N potentiostat (EcoChemie B.V.). A conventional three-electrode cell with an Ag/AgCl (3 M KCl) reference electrode, a gold wire counter electrode, and a polycrystalline gold working electrode (0.11 cm^2 area) was used in all cases. The cell was filled with 1 mM $[Fe(CN)_6]^{3-/4-}$ solutions in 50 mM ACB (pH 4.0 and 5.5) or PB (pH 6.85) and enclosed in a Faraday cage. In EIS experiments, a sine wave of 10 mV amplitude was imposed over the half-wave potential of $[Fe(CN)_6]^{3-/4-}$ species (+0.15 V) at frequencies ranging between 10000 and 0.1 Hz. Impedance data were fitted to a Randles-type circuit (Supporting Information) using the EcoChemie NOVA Frequency Response Analyzer (FRA) 1.8 software.

2.3. Substrate Preparation and Adsorbing Scenarios. Plates used for QCM-D, AFM, and FESEM experiments and the Au electrode (electrochemical measurements) were modified according to the following strategy. First, freshly prepared substrates (cleaned and ordered) were coated with the SAMs by overnight immersion within a 1 mM alkylthiol solution in ethanol. Next, further modification of Au/SAM substrates was achieved by (A) injection of 50 μg mL^{-1} β-LG solutions in 50 mM ACB (pH 4.0 and 5.5) and/or 50 mM PB (pH 6.85) into the QCM-D cell; or (B) immersion of the Au/SAM electrode in these solutions for 24 h.

The apparent pK_a values of the SAMs investigated in this work were reported to fall within the range 5−8 (Table 1).[42−44] Accordingly, in ACB pH 4, charge density should be negligible for the carboxylic acid terminated surfaces (Au/MPA and Au/MUA) but highly positive for Au/AUT. In ACB pH 5.5, whereas Au/MPA and Au/MUA surfaces are expected to bear a still negligible (or a very low) negative charge, Au/AUT should still present a significant positive charge. A different situation is expected in PB pH 6.85: that is, a moderate or relatively low positive charge for Au/AUT and highly negative charge at Au/MPA and Au/MUA.

According to the isoelectric point of β-LG, pI ≈ 5.1,[45] protein molecules are expected to present a significant net positive charge in ACB pH 4 (|pH − pI| ∼ 1.1) and a very low (or even negligible) negative charge in ACB pH 5.5 (|pH − pI| ∼ 0.4). In contrast, a net negative charge (the largest in terms of absolute value) is expected for the biomolecules in PB pH 6.85 (|pH − pI| ∼ 1.7). Thus, according to a simple and qualitative electrostatics basis, the following scenarios are expected (see also the insets of Figure 5): (1) In ACB pH 4, whereas negligible interactions should be established between β-LG and the Au/MPA and Au/MUA surfaces, strong repulsion should occur with Au/AUT. (2) In ACB pH 5.5, negligible interactions are still expected (or in any case a very weak repulsion) with Au/MUA and Au/MPA, but a moderate attraction should be established with Au/AUT. (3) In the last scenario, PB pH 6.85, strong repulsions are expected with the COOH-terminated SAMs, while a moderate-low attraction should be established with Au/AUT.

3. RESULTS AND DISCUSSION

3.1. Characterization of the Substrates. Contact angle measurements revealed the occurrence of significant changes in the polarity of the plates after the deposition of the SAMs (Table 1). Agreeing well with literature data,[11,25,46−50] the surfaces turned more hydrophilic as expected from the introduction of polar groups (X = −COOH and −NH_2). After mounting the samples in the QCM-D cell, these were equilibrated in buffer (prior to the injection of β-LG), resulting in the dissipation of very low amounts of energy in all cases ($\Delta D_n < 2.0 \times 10^{-6}$, Supporting Information) as expected for the formation of rigid alkanethiol films. Surface morphology was inspected by AFM. While the image for bare Au unveiled surface scratches, those were apparently filled after alkanethiol adsorption (Supporting Information). Hence, more flat and smoother surfaces with no significant differences in their topography were observed. Agreeing with that observation, the root-mean-square surface roughness (R_{ms}) decreased from 2.1 ± 0.6 nm for the bare Au,[51] to 1.7 ± 0.2 (Au/MPA), 1.4 ± 0.2 (Au/MUA), and 1.1 ± 0.1 nm (Au/AUT). Interestingly, MPA was the roughest surface, which must be certainly linked to the poorer organization and packing usually achieved by SAMs of short chain thiols. In summary, the Au/SAMs adsorbing platforms used in this work are characterized by their great rigidity, a tunable charge density, and slight differences in thickness and roughness.

dx.doi.org/10.1021/jp409238b | J. Phys. Chem. B 2013, 117, 16565−16576

3.2. Film Flexibility and Surface Aggregation. β-LG adsorption was studied in situ through the simultaneous registration of the fifth overtone normalized frequency ($\Delta f_5/5$) and dissipation factor (ΔD_5) for more than 24 h. Such a long time was given to the system to investigate the slow postattachment structural rearrangements typically occurring in adsorbed proteins. It is worth noting that before calculating the mass uptakes (ρ) through Sauerbrey's equation, the applicability of this model needs to be validated. For these purposes, an analysis of the energy dissipated in the oscillation of the plates is required.

Figure 1 plots the evolution of the flexibility factor (known as K in protein adsorption literature[41] and given here as the ratio between ΔD_5 and $\Delta f_5/5$) for the β-LG films adsorbed under the different scenarios onto Au/MPA (Figure 1A), Au/MUA (Figure 1B), and Au/AUT (Figure 1C). Glasmästar et al. proposed an interesting numerical criterion that permits one to assess whether the rigidity of an adsorbed film is sufficient to allow quantitative analysis through Sauerbrey's model.[33] Accordingly, whenever $K < 0.2 \times 10^{-6}$ Hz^{-1} (dashed dotted lines in the figure), the model can be used as a fair approximation. The results showed that, independently of the underlying alkanethiol, the viscoelastic behavior of β-LG films strongly depended on the working pH. With the exception of the Au/MPA/β-LG film (for which the limit was just barely reached), Figure 1 presents flexibilities well above Glasmästar's limit at pH 5.5. In great contrast, working in slightly acidic and/or nearly neutral pH resulted in film flexibilities far below this value in all cases. Remarkably, under the latter conditions, the Au/MPA/β-LG film was slightly more flexible than its counterparts.

Hence, whereas the quantitative analysis of the QCM-D data obtained at pH 4.0 and 6.85 through Sauerbrey's equation is valid, the great flexibility exhibited by the films at pH 5.5 must result in a large overestimation of the mass uptakes due to viscous effects. In any case, and despite that it is clear that these are far from representing a pure protein+trapped water load, they have been presented yet for their qualitative discussion in the context of aggregation phenomena. Another conclusion is that the long chain SAMs (C_{11}) are more prone than MPA (C_3) to accommodate β-LG films, which are either more flexible (in the surroundings of the pI) or more rigid (when the pH is far from this value). The restricted changes evidenced in the viscoelasticity of the Au/MPA/β-LG films might be the consequence of the lower thickness and the slightly higher roughness unveiled in section 3.1 for its underlying substrate (Au/MPA).

The reliability of the AFM technique for the direct assessment of the orientation and conformation of adsorbed proteins is limited by several factors. In the first place, AFM in liquid suffers from a poor lateral resolution, large contributions of hydrodynamic effects, and enhanced sensitivity to sample-tip interactions, to be able to resolve structural motifs. Second, although high-resolution AFM in air has been able to image individual structural domains,[52] it is not clear whether the "dry" images are representative of the proteins in solution. Accordingly, AFM images were taken in air only with the purpose of assessing the large-scale aggregation of β-LG on these surfaces.

Figure 2 displays the AFM topographic images obtained for the Au/SAM/β-LG plates studied in Figure 1. Independently of the supporting substrate, large bodies with diameters between 100 and 400 nm dominated the images when β-LG was

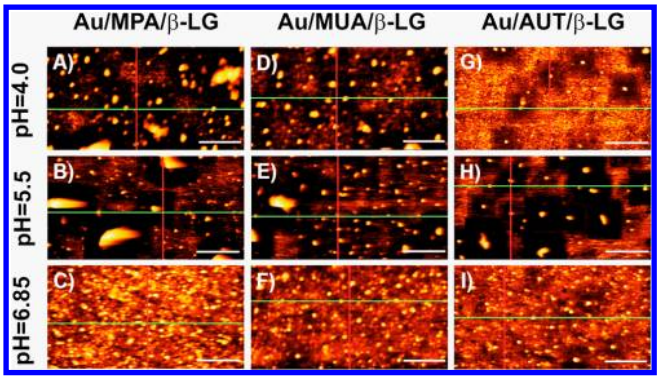

Figure 2. AFM images taken in air for Au/MPA/β-LG (A–C), Au/MUA/β-LG (D–F), and Au/AUT/β-LG (G–I) quartz plates prepared from 50 μg mL^{-1} β-LG solutions in 50 mM ACB pH 4.0 (A, D, G), 50 mM ACB pH 5.5 (B, E, H), and 50 mM PB pH 6.85 (C, F, I) in the previous section. The plates were dried under N_2 before measurements. Height profiles along the colored lines can be found in the Supporting Information. Scale bar = 1 μm.

adsorbed close to its pI (Figure 2B, E, and H), which is in excellent agreement with the great viscoelasticity exhibited by the films in Figure 1. In addition, no sign of the underlying Au was recognizable in the background, which indicates that these are also relatively tall. In line with this view, the height profiles extracted along the colored lines confirmed an increase in the maximum height after the deposition of β-LG of at least 4 times (Supporting Information). Under the present scenario (ACB pH 5.5), the repulsion between neighbor β-LG molecules (bearing a very low charge) should be almost negligible, which would allow other non-Coulombic forces to induce their association into large particles.

In contrast, a much lower degree of aggregation was evidenced at near neutral pH (Figure 2C, F, and I). Spherical particles of about 100 nm diameter were identified onto the three substrates. The microstructure of Au is clearly recognized in the background (grain size around 40 nm), which means that the particles are much shorter when compared to those observed at pH 5.5. These findings are in excellent agreement with the height profiles extracted from the images and the enhanced rigidity exhibited in Figure 1. Remarkably, with the notable exception of the Au/AUT/β-LG film, aggregation was slightly more significant at pH 4 (Figure 2A, D, and G). This behavior is surprising because the strong repulsion between β-LG neighbor molecules (positively charged) should prevent, at least partially, their association via weak forces. On the other hand, the negligible aggregation observed at Au/AUT/β-LG is in line with the low flexibility of this film, which could be attributed to the strong electrostatic repulsion established between the Au/AUT substrate and the single molecules, and/or large aggregates, of β-LG.

In addition to the height profiles, other statistical parameters such as the average height (H_{AV}) and the root-mean-square surface roughness (R_{MS}) were extracted from the images (Table 2). The results completely agreed with the qualitative description made above: that is, the highest values of H_{AV} and R_{MS} were obtained from Figure 2A, B, D, E, and H. Accordingly, the values of R_{MS} and flexibility measured at pH 4 for Au/MPA/β-LG (10.8 nm and 0.145×10^{-6} Hz^{-1}) and Au/MUA/β-LG (4.1 nm and 0.125×10^{-6} Hz^{-1}) were also slightly larger than those for Au/AUT/β-LG (3.2 nm and 0.113×10^{-6} Hz^{-1}). These differences agree with the presence of large

dx.doi.org/10.1021/jp409238b | J. Phys. Chem. B 2013, 117, 16565–16576

Table 2. Statistical Parameters, the Root-Mean-Square Surface Roughness (R_{ms}), and the Average Height (H_{AV}), Calculated from the AFM Images in Figure 2 by Means of the Software Gwyddion 2.25

surface	R_{ms}/nm	H_{AV}/nm
Au/MPA/β-LG[a]	7.4 ± 0.7	45 ± 1
Au/MPA/β-LG[b]	11.9 ± 0.9	64 ± 2
Au/MPA/β-LG[c]	2.1 ± 0.5	8 ± 1
Au/MUA/β-LG[a]	3.5 ± 0.4	36 ± 1
Au/MUA/β-LG[b]	7.9 ± 0.6	73 ± 1
Au/MUA/β-LG[c]	1.5 ± 0.3	4 ± 1
Au/AUT/β-LG[a]	1.7 ± 0.2	12 ± 1
Au/AUT/β-LG[b]	4.9 ± 0.4	31 ± 1
Au/AUT/β-LG[c]	1.1 ± 0.1	4 ± 1

[a]ACB pH 4. [b]ACB pH 5.5. [c]PB pH 6.85.

protein aggregates at the noncharged surfaces (X = COOH) and their notable absence on the Au/AUT surface. As discussed above, the repulsive interactions felt by single β-LG molecules (or their aggregates) in their way to the surface may limit the aggregation in this case.

It is worth noting that, at every pH, the highest values of R_{MS} were measured always for the Au/MPA/β-LG film, which must be certainly linked to the higher roughness of the underlying substrate. Accordingly, the viscoelastic stabilization of this film at pH 5.5 could be explained through a mechanism of partial filling of the defects at the MPA layer with protein. Thereby, surface aggregation will be reduced, and the film would behave more rigidly than those deposited on the more smooth and flat Au/MUA and Au/AUT substrates.

Sample regions scanned by AFM have typical dimensions of micrometers, and, sometimes, they are not representative of a whole surface. In addition, the interaction of the tip with the sample can still alter the nature of the images. In such a context, reliable conclusions require a comparison with the data coming from a noninvasive technique. Accordingly, the Au/SAM/β-LG plates were subsequently studied by FESEM (Figure 3). As suggested by AFM images, the results confirmed a relatively important impact of aggregation at pH 5.5 (Figure 3B, E, and H) and pH 4 (Figure 3A, D, and G). As seen in the images, these films contain large aggregated particles that are far from behaving rigidly during the oscillations just as demonstrated by the viscoelastic data in Figure 1.

A careful inspection of these particles in secondary electrons mode (see figure insets) revealed the presence of bright three-dimensional (3D) structures with size between 1 and 12 μm (much larger than those observed in Figure 2) over the three substrates. Also agreeing with the AFM data, the lowest degrees of aggregation were observed at pH 6.85 (Figure 3C, F, and I) for which the major part of the plates seemed to be covered with a homogeneous layer of β-LG. Nonetheless, oppositely to the small spherical particles shown in Figure 2C, F, and I, axial rod-shaped structures with a length of micrometers, and certain 3D character, were found in the images.

Different pathways can be called to explain the formation of the structures imaged by AFM and FESEM: (a) particle growth in solution and subsequent deposition on the surface, (b) direct growth on the surface upon 2D seeds through a dewetting-driven effect, and (c) combinations of both mechanisms. Changes in the brightness of FESEM images often reflect changes in the thickness/height of the investigated films. The 3D particles detailed in the insets of Figure 3A, B, D, E, G, and H present darker areas within their own cluster structure, which likely represent a lowered particle thickness.

The association of β-LG molecules in oligomers has been reported to occur in solution when high concentrated solutions with pH around the pI are used.[53] Alternatively, very recent results have also pointed to the destabilization of proteins (and the acceleration of aggregation in solution) when transient air–

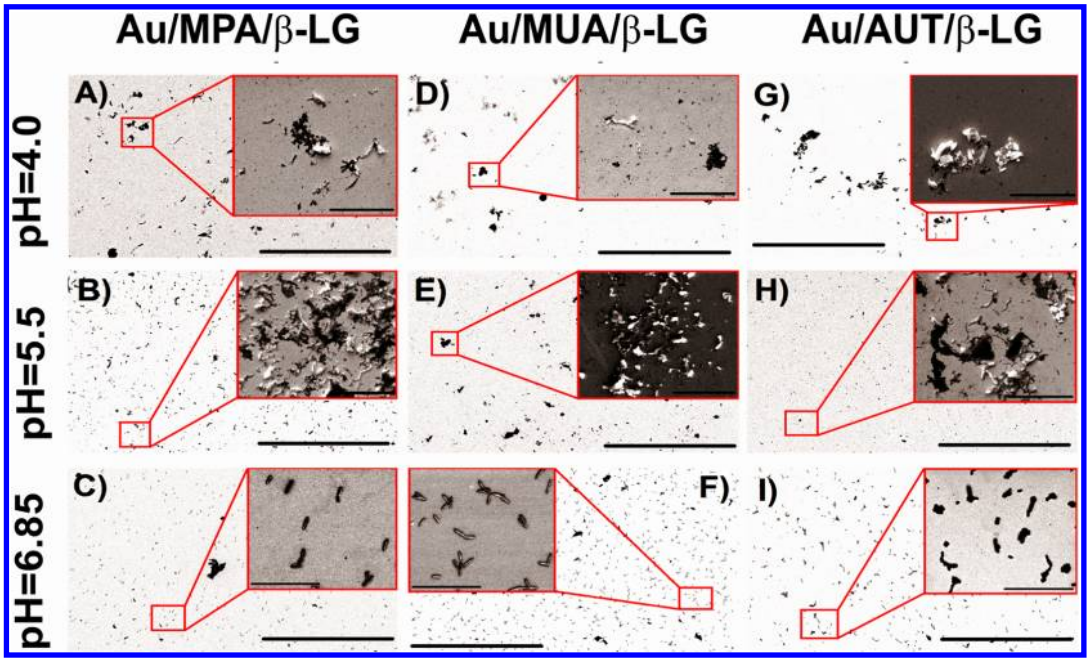

Figure 3. SEM pictures obtained for Au/MPA/β-LG (A–C), Au/MUA/β-LG (D–F), and Au/AUT/β-LG (G–I) QCM-D quartz plates prepared from 50 μg mL^{-1} β-LG solutions in 50 mM ACB pH 4.0 (A, D, G), 50 mM ACB pH 5.5 (B, E, H), and 50 mM PB pH 6.85 (C, F, I). Backscattered (BSED) and secondary electrons (SE) modes were used for the main images and the insets, respectively. The scale bars are 100 μm (main images) and 10 μm (insets).

dx.doi.org/10.1021/jp409238b | J. Phys. Chem. B 2013, 117, 16565–16576

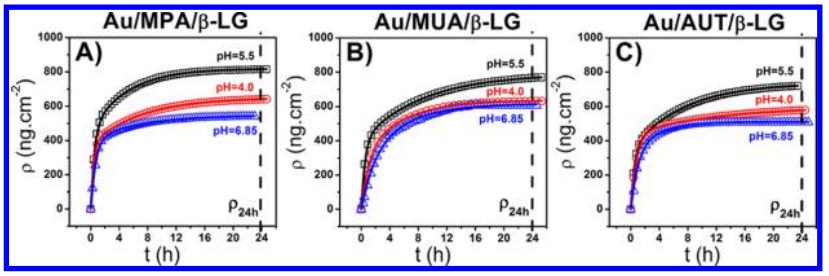

Figure 4. Changes in surface mass density, calculated from $\Delta f_5/5$ data using Sauerbrey's equation, for the adsorption of β-LG onto Au/MPA (A), Au/MUA (B), and Au/AUT (C) surfaces upon injection of 50 μg mL^{-1} solutions in 50 mM ACB pH 5.5 (□), 50 mM ACB pH 4.0 (red ○), and 50 mM PB pH 6.85 (blue △). The straight lines represent the fitting of the experimental data to eq 1.

liquid interfaces as those generated, for instance, by continuous stirring or bubbling aeration are involved.[54] Rabe et al. studied the dynamics of adsorption of 3D protein clusters onto different surfaces by means of the Förster resonance energy transfer (FRET) technique.[2] A mechanism of growth in solution followed by deposition and subsequent spreading on the surface was proposed to explain their results. It is worth noting that a similar behavior was suggested for the adsorption of β-LG onto Au/AUT substrates coated with a bilayer of polystyrene sulfonate and colloidal chitosan (Au/AUT/pSS/Chit).[31] In that work, large clusters characterized with darker areas, which were described as regions where the aggregates would be already semispread on the surface, were also found. The similarities with the FESEM images herein obtained at pH 5.5 strongly suggest that these particles could have followed an analogous fate.

On the other hand, the occurrence of rod-shaped aggregates at pH 6.85 is in great contrast with the strong electrostatic repulsion expected between the negatively charged protein molecules. Guzzi et al. studied, also by means of SEM, the morphology of different aggregates formed after casting drops of a diluted, and prefiltered, β-LG solution onto different surfaces.[36] Isolated in small regions, which apparently dried in the form of microdroplets, they found aggregates with different morphologies. Among them, rod-shaped particles, similar to those in our images, were observed only at pH 2 (a similar scenario of strong repulsion expected between protein molecules). In fact, the formation of these aggregates was shown more connected to the particularities of surface dewetting than to any process in solution.

In this respect, the formation of microdroplets seems to play a key role, as local protein concentrations can achieve the critical values required to form the corresponding seeds. Hence, the small amounts of rod-shaped aggregates observed in our experiments could be also related to the particularities of local dewetting phenomena. At pH 4, a homogeneous protein layer covers vast areas of the surface, but one can still recognize isolated semispread particles and/or rod-like structures. A combination of both mechanisms then can be proposed in this case due to (1) a likely insufficient pH gradient to prevent completely from aggregation processes in solution (|pH − pI| = 1.1 vs 1.7 at pH 6.85) or their stimulated formation due to solution stirring; and (2) formation of seeds, and their further growth into rods, boosted by dewetting processes in microdroplets.

3.3. Adsorption Kinetics and Mass Uptakes. Figure 4 displays ρ versus t plots calculated from the $\Delta f_5/5$ data by means of Sauerbrey's equation. Exponential curves without peaks or overshootings, which are usually regarded as indicative of irreversible adsorption,[34,35] were obtained for every scenario. Such a behavior was found before for the adsorption of β-LG onto silica[55] and colloidal chitosan,[31] hemoglobin onto citrate,[56] and α-casein onto alkylthiol SAMs,[9] and suggests negligible changes in the affinity of the adsorbed proteins toward the surface (e.g., caused by changes in their orientation) or their exchange with solution proteins. In fact, rinsing the plates with fresh buffer at the end of the experiments confirmed the negligible desorption of β-LG in all of the cases (see the Supporting Information).

By further plotting the adsorption rate ($d\rho\ dt^{-1}$) versus ρ, the existence of two linear domains characterized by different rate constants was unveiled (Supporting Information). The quasi-spherical shape of β-LG, together with the evidence collected on its irreversible adsorption, allowed discarding the establishment of meaningful orientational transitions. Thereby, the variations in the second region of the plots can be mostly attributed to changes in the conformation of the adsorbed macromolecules. This is an important aspect (further discussed in section 3.4), because conformational transitions in proteins often lead to a partial (or complete) unfolding of the native structure and its subsequent loss of activity. Fitting the experimental data to eq 1 (solid lines in Figure 4) supplied excellent results with correlation factors $R^2 \geq 0.9995$ in all cases.

Table 3 presents the fitting parameters obtained for each kinetic domain. It is noteworthy that k_2 was consistently about

Table 3. Parameters Obtained after Fitting the Experimental Data in Figure 4 to Equation 1

surface	$k_1 \times 10^{-6}$/ cm min^{-1}	$k_2 \times 10^{-4}$/ cm min^{-1}	$\lvert A_1 \rvert$ /cm^2 ng^{-1}	$\lvert A_2 \rvert$/ cm^2 ng^{-1}
Au/MPA/β-LG[a]	5.8	1.6	0.0036	0.0027
Au/MPA/β-LG[b]	4.4	1.2	0.0035	0.0018
Au/MPA/β-LG[c]	5.0	0.9	0.0047	0.0030
Au/MUA/β-LG[a]	8.2	0.4	0.0032	0.0031
Au/MUA/β-LG[b]	6.2	1.2	0.0025	0.0025
Au/MUA/β-LG[c]	5.4	0.2	0.0039	0.0027
Au/AUT/β-LG[a]	1.7	0.8	0.0062	0.0023
Au/AUT/β-LG[b]	8.2	1.0	0.0029	0.0026
Au/AUT/β-LG[c]	8.0	0.5	0.0052	0.0032

[a]50 mM ACB pH 4. [b]50 mM ACB pH 5.5. [c]50 mM PB pH 6.85.

1 order of magnitude greater than k_1. This finding is in excellent agreement with that reported for the adsorption of β-LG onto Au/AUT/pSS/Chit[31] and suggests that the conformational changes undergone by adsorbed proteins occur much faster than their attachment to the surface. The latter then may control the kinetics of the whole adsorption process. This is, additionally, in line with previous demonstrations that the

dx.doi.org/10.1021/jp409238b | J. Phys. Chem. B 2013, 117, 16565−16576

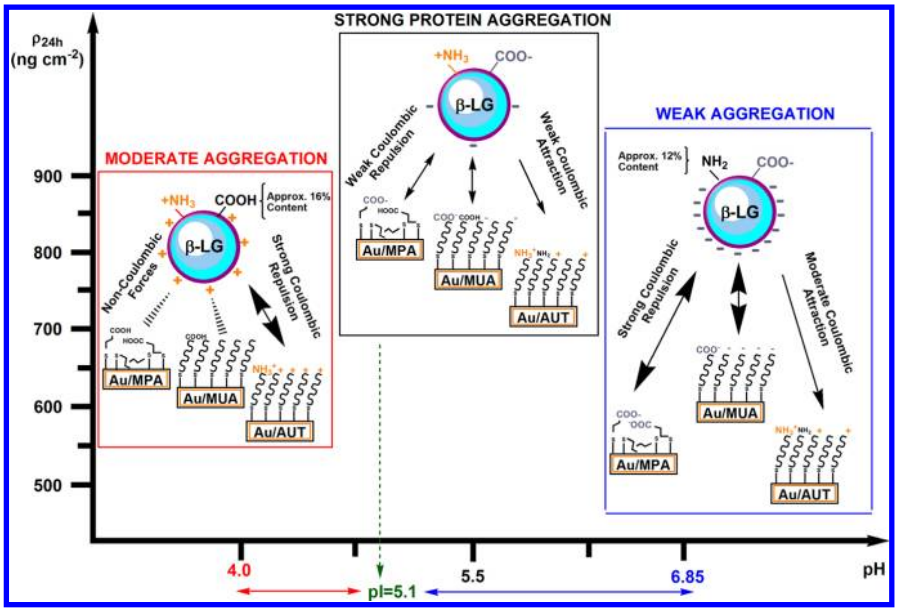

Figure 5. Correlation between the mass uptakes registered after 24 h on the three different substrates (derived from data in Figure 4) and the solution pH of the investigated buffers. The insets illustrate the charge at surface and protein and the Coulombic forces for each scenario proposed. The arrows indicate the nature of the interaction (double-sided, repulsion; single-sided, attraction) and intensity (thicker point arrows indicate higher intensity). For simplicity, protein-bound water has not been considered.

native conformation of supported proteins can be stabilized or kinetically trapped, from concentrated solutions, through sterical hindrance.[57] Further analysis of k_1 revealed that the slowest attachment of β-LG occurred onto Au/AUT at pH 4 (1.7×10^{-6} cm min^{-1}) as well as onto Au/MUA, and Au/MPA, at pH 6.85 (5.4×10^{-6} cm min^{-1} and 5.0×10^{-6}, respectively). The strongly repulsive protein−surface Coulombic forces established under these conditions are thought to determine the slower saturation of the available sites by single proteins and/or large aggregates.

In this respect, the process turned significantly faster (with k_1 in the range $(6-8) \times 10^{-6}$ cm min^{-1}) when one of either the substrate (Au/MUA at pH 4 and Au/AUT at pH 6.85) or the protein (β-LG at pH 5.5) presented a negligible charge. These findings contrast sharply with recent surface plasmon resonance (SPR) and fluorescence recovery after photobleaching (FRAP) data illustrating a negligible interaction, and subsequent adsorption, of charged ferritin (and bovine serum albumin) with several uncharged solid lipid bilayers.[26] In fact, contradictory results have been reported in the literature for albumin adsorption pointing to its control by either electrostatic or hydrophobic forces.[9,58] The kinetic data and the shape of the curves obtained for β-LG under the previously referred conditions constitute evidence that its adsorption onto Au/SAMs cannot be explained only by the consideration of the net protein charge and the Coulombic forces established with the substrates. To further understand this result, a balance between these and other non-Coulombic interactions has to be necessarily considered.

Because of the hydrophilic nature of the surfaces investigated, hydrophobic interactions are expected to be negligible, and, thus, H bonding emerges as the most relevant among all of these forces. At this point, it should be noticed that approximately 12% of the residues in the β-LG sequence bear amino groups (lysine, Lys; arginine, Arg; and histidine, His) versus a 16% substituted with carboxyl groups (aspartic and glutamic acids: Asp and Glu).[59] Seemingly, the formation of H-bond networks between β-LG and the AUT-modified surface should be slightly favored at any pH. However, such a small difference in the chemistry of the protein was not reflected on the values of k_1 due to the strongest effects of electrostatics and aggregation. On the other hand, the slowest attachment of β-LG was systematically observed onto the Au/MPA surface, which is likely ascribed to its enhanced roughness. In fact, rough surfaces usually present enhanced resistance to protein adsorption due to surface exclusion and other effects.[60]

Remarkably, the kinetics in the second region showed no apparent dependence on electrostatics. Rearrangements were systematically faster when β-LG was adsorbed from solutions buffered at pH 5.5 ($k_2 \geq 1.0 \times 10^{-4}$ cm min^{-1}). Albeit a detailed assessment on the stability of the adsorbed proteins is presented in the next section, this observation seems to confirm a behavior analogous to that reported on Au/AUT/pSS/Chit surfaces:[31] that is, conformational changes produced under strong self-aggregation advance in the sense of kinetically trapping, or reinforcing, the folded states of β-LG via protein−protein lateral forces. Interestingly, the fastest rearrangements at every pH occurred onto the MPA surface. Roughness is thought to confer a certain degree of physical entrapment to the proteins deposited within defects so that their structural relaxation is physically restricted.

One way to scrutinize the possible contribution of H-bonding interactions to the adsorption process involves the comparison of k_2 for Au/MUA and Au/AUT when far from the protein's pI. In this respect, and agreeing with the more favored formation of H bonds expected on the Au/AUT substrate, slightly faster conformational transitions were found on it at pH 4 ($k_2 = 0.8 \times 10^{-4}$ vs 0.4×10^{-4} cm min^{-1} for Au/MUA) and pH 6.85 ($k_2 = 0.5 \times 10^{-4}$ vs 0.2×10^{-4} cm min^{-1}). As a major conclusion, it seems that weak non-Coulombic forces are more important than their Coulombic counterparts in the conformational changes followed by adsorbed β-LG. Regarding the steric factors, slightly lower values were systematically obtained at the second step ($|A_2|$). Low values of $|A|$ often represent the

dx.doi.org/10.1021/jp409238b | J. Phys. Chem. B 2013, 117, 16565−16576

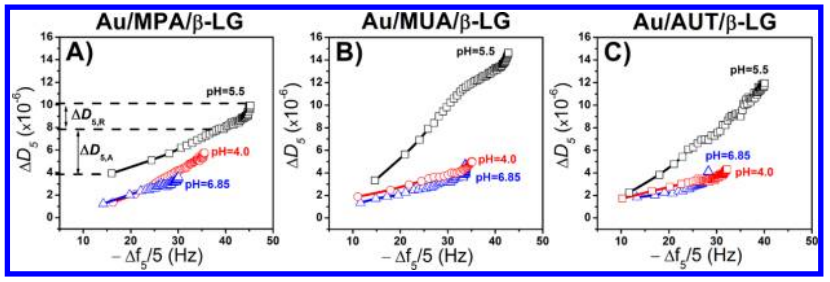

Figure 6. Correlation between energy dissipation (ΔD_5) and frequency shift ($\Delta f_5/5$) data extracted from the QCM-D experiments for the different Au/SAM/β-LG films (A−C) adsorbed from 50 mM ACB pH 4 (red ○), ACB pH 5.5 (□), and PB pH 6.85 (blue △).

formation of compact and well-packed structures.[15] Hence, considering that β-LG films are more populated and dense at higher coverage, these results seem quite reasonable. It is also noticeable that the lowest values of $|A_2|$ were obtained at pH 5.5 for which a boosted aggregation of protein has been unveiled from microscopy and flexibility data. Also in line with this view, maximum values were reached at pH 6.85 ($|A_2| \geq 0.00275$) under which minimum aggregation of protein has been proved.

The mass uptakes registered after 24 h adsorption (ρ_{24h} in Figure 4) have been correlated in Figure 5 to the pH of the solutions and the impact of aggregation (as deduced from the data in Figures 1−3). In line with the strong aggregation disclosed at pH 5.5, the largest loads of protein were also recorded under these conditions (black inset in Figure 5) with up to 815 ng cm^{-2} attained onto the Au/MPA surface. However, as clearly evidenced in Figures 1−3, these results are strongly interfered by viscoelastic phenomena and cannot be taken as quantitative. Therefore, their subsequent discussion in these terms would be worthless. Concomitant with the weak aggregation observed at pH 6.85 (blue inset), the lowest loads of protein were also detected under these conditions. For instance, ρ_{24h} = 547 and 612 ng cm^{-2} were achieved onto Au/MPA and Au/MUA, respectively. In addition to the weak aggregation, the strong protein−surface electrostatic repulsion expected in these cases certainly contributed to limit the deposited mass.

Even though aggregation and Coulombic forces appear to be the main factors determining the values of ρ_{24h} so far, the fact that the lowest value recorded at this pH occurred onto the Au/AUT surface (509 ng cm^{-2}) questions this view because surface−protein attractive forces would be expected to favor the deposition of larger protein loads. In this respect, one could argue on the low/moderate charge density borne by this surface under these conditions (as described in section 2.2). However, the kinetic data obtained at pH 6.85 (Table 3) illustrated how, whereas the fastest attachment of β-LG did actually occur on Au/AUT (which confirms that charge density was still significant), conformational transitions were, on the contrary, much slower on this substrate. Consequently, ρ_{24h} must be regarded as the result of a balance between the surface attachment (mainly affected by electrostatics) and the posterior conformational changes at the protein (apparently controlled by non-Coulombic forces).

As it will be better explained in section 3.4, refolding of adsorbed β-LG molecules could be slightly restricted on this surface, thus allowing the accommodation of lower amounts of protein despite the most favorable electrostatic scenario. At pH 4 (red inset in Figure 5), ρ_{24h} values were slightly higher. This might be the consequence of the stronger impact of aggregation evidenced above. Although an electrostatic framework similar to that described for Au/AUT at pH 6.85 (characterized by the establishment of weak surface−protein Coulombic forces) could be also expected to govern the adsorption onto Au/MPA and Au/MUA, much higher uptakes were measured in these cases (641 and 633 ng cm^{-2}, respectively). Whether the small difference obtained for both surfaces is significant or just due to a slightly enhanced capability to accommodate proteins by the disorganized and rough MPA SAM is difficult to assess.

On the other hand, the minimum uptake at this pH was measured onto Au/AUT (579 ng cm^{-2}), which seems determined by the combination of a strong surface−protein repulsion and the slow conformational changes followed by β-LG on this surface. As discussed above, the minimum value of ρ_{24h} was 509 ng cm^{-2} for Au/AUT at pH 6.85. Interestingly, this is almost twice the 270 ng cm^{-2} calculated by Wahlgreen and Arnebrant for a hexagonally close-packed monolayer (ML) of β-LG assembled on flat surfaces.[61] Therefore, as suggested by the SEM evidence, an initial hypothesis is that β-LG would adsorb in multilayers from the concentrated solutions used in these experiments. Nonetheless, the contributions of viscoelasticity and trapped water need to be considered before validating this claim. In this respect, the overestimation of the mass uptakes measured with the QCM-D can vary between about 20% (only wet contribution) and 50% (water + viscoelastic effects) of the total mass.[62]

In the aforementioned work using Au/AUT/pSS/Chit substrates, very diluted solutions of β-LG (~2.5 μg mL^{-1}) were required to limit its adsorption to about one ML.[31] This led to an uptake of 390 ng cm^{-2}, which overestimates the theoretical ML value by about 31% (or even more, given that ML adsorption onto a nonflat biopolymer-decorated surface would likely involve less than 270 ng cm^{-2}). Even considering that the uptakes presented in Figure 5 for pH 6.85 could be overestimated by 40%, the values obtained after correction will lie between 300 and 360 ng cm^{-2} (still above the ML level), which seems to validate the hypothesis of adsorption in multilayers even at those scenarios characterized with the minimum aggregation.

3.4. Protein Stability. Deeper insights on the conformational stability of adsorbed β-LG can be obtained through the analysis of ΔD_5 versus $\Delta f_5/5$ plots (Figure 6). With the decrease of the vibrating frequency caused by adsorption, ΔD_5 increased along two linear domains characterized by different slopes (attachment and rearrangements). While the most pronounced changes took place always in the first region, the second was characterized by small changes in ΔD_5 occurring in a very narrow range of frequencies (Figure 6A). From the little impact caused by the structural rearrangements in the viscoelasticity of the films, it seems that they did not promote,

dx.doi.org/10.1021/jp409238b | J. Phys. Chem. B 2013, 117, 16565−16576

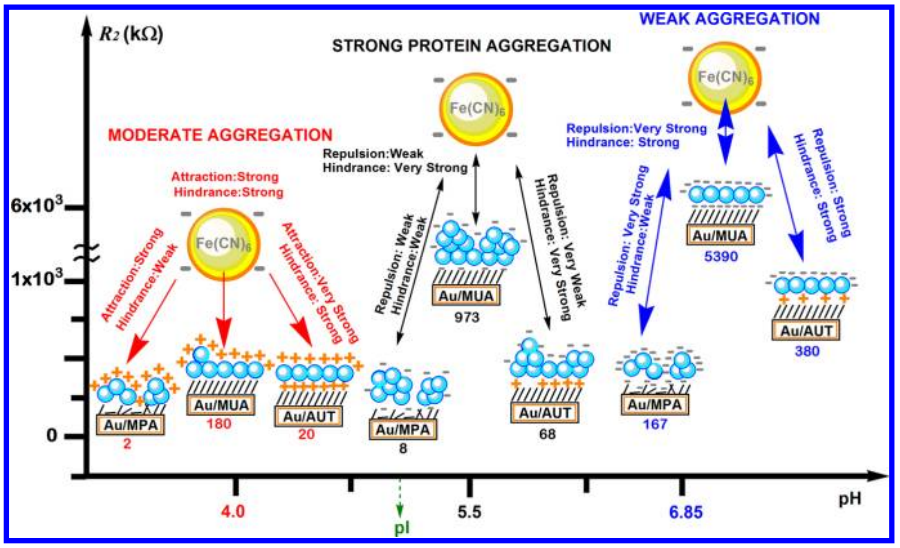

Figure 7. Comparison of the ET barriers obtained for Au/SAM/β-LG electrodes in the different electrolytes containing 1 mM $[Fe(CN_6)]^{3-/4-}$ (red, black, and blue zones). The barriers are given in the form of an apparent charge transfer resistance (R_2), which derives from fitting the EIS spectra to a Randles-type circuit. Blue spheres represent individual or aggregated β-LG molecules. The represented coverage is based on the uptakes presented in Figure 5. Protein net charge in each situation is indicated by surrounding "−" (gray) or "+" (orange) symbols. Golden spheres represent the negatively charged $[Fe(CN_6)]^{3-/4}$ solution species. The arrows indicate the nature of the Coulombic interactions (double-sided, repulsion; single-sided, attraction) and intensity (thicker arrows indicate higher intensity). The charge of the underlying SAM is also shown. For simplicity, protein-bound water has not been considered.

in any case, additional adsorption of meaningful amounts of β-LG.

The unfolding of proteins has been characterized by an increase in the population of exposed hydrophobic and hydrogen bonded structural motifs (β-sheets and strands) together with a decrease of the hydrophilic ones (α-helices, β-turns, and random coils).[63] The spreading of a adsorbed protein on its support, as a result of structural relaxation, is expected to increase its footprint, which must be necessarily accompanied by an increase in the rigidity of the films, that is, by a decrease in the shift of the dissipation factor in the second region (ΔD^R). In great contrast, Figure 6 exhibits a negligible or slight increase in $\Delta D_5{}^R$ for all of the investigated cases. On the other hand, a different type of conformational transition, which, oppositely, raises the population of exposed hydrophilic elements, has been also reported for β-LG,[31] and other proteins, when adsorbed from concentrated solutions under scenarios of enhanced aggregation.[63]

Instead of promoting unfolding, these transitions (powered by strong protein−protein lateral forces) reinforce the folded states, which must reduce the protein footprint and produce an increase in $\Delta D_5{}^R$ analogous to those observed in Figure 6. Another interesting point is the higher slopes exhibited in the second domain. This behavior indicates that the conformational transitions proceed much faster than the attachment to the surface, which, by the way, confirms the kinetic results in Table 3. The short and fast variations of $\Delta D_5{}^R$ registered in Figure 6 are compatible with a major preservation of the native state of β-LG, or even its slight refolding, upon adsorption onto the Au/SAM substrates. In this line, the largest values of $\Delta D_5{}^R$ were observed in the context of strong aggregation, that is, Au/MPA/β-LG ($\Delta D_5{}^R = 1.1 \times 10^{-6}$) and Au/MUA/$\beta$-LG films ($\Delta D_5{}^R = 1.3 \times 10^{-6}$) at pH 5.5 (black data in Figure 6A and B). These changes suggest a significant decrease in the protein's footprint driven by the previously referred mechanism.

Very low or negligible changes in $\Delta D_5{}^R$ (indicating that adsorbed proteins did not follow significant unfolding/refolding) were also measured for the Au/MPA/β-LG films under scenarios of reduced aggregation (red and blue curves in Figure 6A). These results are attributed to the physical entrapment of β-LG within the more defective and rough structure of MPA. In fact, an analogous stabilization of the folded states has been shown before for proteins entrapped within layer-by-layer (LbL) multiassemblies, solid porous nanocomposites, and other 3D matrixes.[64] In addition to aggregation and physical entrapment, the hydrophilic character of the investigated substrates may also contribute to the great conformational stability of adsorbed β-LG. In this sense, favorable electrostatics and H-bonding could favor the enclosure of hydrophobic parts of β-LG within its core reinforcing the folded state.

It was discussed above that the small differences in the content of $-NH_2$ and $-COOH$ groups in the β-LG sequence could lead to a slightly favored H-bonding on the Au/AUT surface. These interactions with the outer sphere of the protein (mostly hydrophilic) should stabilize, or even refold, the native state, which could be argued to induce a reduction in the footprint and a further increase in $\Delta D_5{}^R$. Nevertheless, at pH 4, the value of $\Delta D_5{}^R$ measured for Au/AUT/β-LG was slightly lower (0.8×10^{-6}) than that for Au/MUA/β-LG (0.9×10^{-6}). This behavior seems to be determined by the lower amounts of β-LG adsorbed onto Au/AUT (i.e., lower lateral pressure) in the context of the strong electrostatic repulsion established between them. In fact, at pH 6.85 (when attractive interactions are established with Au/AUT and repulsive with Au/MUA), the value obtained for the first one was slightly higher ($\Delta D_5{}^R = 1.2 \times 10^{-6}$ vs 0.9×10^{-6}).

3.5. Film Permeability. The permeability of protein films to water and solution species can be evaluated by means of electrochemical techniques. This information is valuable because it allows validating some of the conclusions made in previous sections. To this end, the electrochemical response of bare Au, Au/SAM, and Au/SAM/β-LG electrodes was registered in the buffer solutions containing 1 mM [Fe-

dx.doi.org/10.1021/jp409238b | J. Phys. Chem. B 2013, 117, 16565−16576

$(CN)_6]^{3-/4-}$ (a typical probe in electron transfer, ET, studies[65] and widely used in electrochemical biosensors[66]). EIS is a more sensitive, nondestructive, and straightforward technique than CV for the evaluation of ET barriers so that, given the general agreement found between them, just the impedance data are discussed (CVs can be found in the Supporting Information). In this respect, ET barriers are typically reflected in Nyquist plots as semicircles that appear in the range of high-medium frequencies (where an apparent charge transfer resistance, R_2, controls the total impedance). Wide semicircles and concomitantly high values of R_2 then are related to low values of the apparent ET rate constant (*kapp*).[46] R_2 was determined in the investigated systems by fitting the Nyquist plots to a Randles-type equivalent circuit.

The response of Au and Au/SAM electrodes can be summarized as follows: (A) very low barriers were found for bare Au in any of the electrolytes investigated ($R_2 \approx 1-8$ kΩ), which is evidence of fast ET; and (B) the response of the Au/SAM electrodes strongly depended on their surface charge at a given pH; that is, it depended on the intensity and type (repulsive/attractive) of electrostatic interactions established with the negatively charged probes. Figure 7 compares the R_2 data obtained for the Au/SAM/β-LG electrodes under the different scenarios. It is meaningful to note that the apparent ET barriers obtained through this approach include contributions from both the mass transport (which might be affected by the compactness and porosity of the films) and the intermolecular interactions established with the probe.

In this context, the deposition of β-LG onto Au/SAMs is expected to change the diffusion of the probe across the different assemblies due to steric hindrance and electrostatic effects. The research conducted in the last decades within the field of LbL assembly has evidenced the existence of preferential pathways toward the supporting substrate in these films, which can be physically blocked after deposition of a critical number of layers.[67] Analogously, the deposition of a high coverage film or large aggregates of β-LG onto the SAMs could hinder the penetration of solvent and probes into the films. In parallel, the establishment of repulsive/attractive probe−protein Coulombic interactions is also expected to influence their permeability to the probe species.[46]

As shown in Figure 7, the lowest values of R_2 were systematically obtained for the Au/MPA/β-LG electrodes. Such a biased response was also observed within the Au/SAM series and strongly agrees with the more disorganized and defective MPA films facilitating the mass transport across them. On the other hand, the maximum values of R_2 were achieved for (1) Au/MUA/β-LG at pH 5.5 (973 kΩ), (2) same at pH 6.85 (5391 kΩ), and (3) Au/AUT/β-LG at pH 6.85 (379 kΩ). In case (1), the small charge borne by protein molecules and the weak repulsion subsequently established with the probes should not be expected to complicate their incorporation into the film. However, the strong aggregation of β-LG evidenced under these conditions and the significant steric hindrance introduced may determine the high ET barrier measured.

In (2), the highly negative charge density at both layers (the outermost protein layer and at the underlying MUA) may explain the huge resistance measured despite the easier mass transfer expected in the absence of significant aggregation. Oppositely, in (3), the positive charge at the underlying AUT reduces the net negative interfacial charge leading to a much lower value of R_2. As illustrated in the insets of Figure 7, the obtained ET barriers can be explained, in all cases, in terms of the combination of electrostatic forces and steric hindrance felt by the redox probes and, in general, agree quite well with the conclusions made from Figures 1−3.

4. CONCLUSIONS

The adsorption and stability of a model spheroprotein onto rigid and hydrophilic Au/SAM substrates (of tunable charge) were investigated in the context of different experimental scenarios. Through this material choice, the contribution of orientational transitions to the rearrangements typically occurring after attachment of proteins to a surface can be neglected, and the unfolding of the native structure is also more limited. In principle, and through these simplifications, the particularities of the investigated issues could be correlated more easily to the type of intermolecular forces ruling under the different experimental scenarios. However, the results herein obtained illustrate that adsorption phenomena remain relatively complex even when rationalized attempts are made for its deconvolution.

The results seemingly point that self-aggregation and electrostatics are the main forces determining the amounts of loaded protein (and its conformational stability). However, by analysis of those scenarios in which a weak/negligible aggregation and electrostatics are expected, it was revealed that other non-Coulombic forces, such as H-bonding, may also influence some of the particularities of the process. This is in contrast with the common idea in the literature that the electrostatic interactions established between a polarized substrate and an oppositely charged protein solely govern the adsorption processes. Thus, it can be postulated that, for the investigated system, adsorption emerges as the balance between these and other weaker intermolecular forces established under the given experimental conditions.

■ ASSOCIATED CONTENT

Supporting Information

(A) Sauerbrey's equation, (B) RSA theory, (C) Randles-type equivalent circuit, (D) electrochemical response of Au/SAM electrodes, (E) additional figures and tables, and (F) references. This material is available free of charge via the Internet at http://pubs.acs.org

■ AUTHOR INFORMATION

Corresponding Authors

*Tel.: (+351) 220402643. Fax: (+351) 226082959. E-mail: jpina@fc.up.pt (J.M.C.).
*E-mail: jborges@fc.up.pt (J.B.).

Notes

The authors declare no competing financial interest.

■ ACKNOWLEDGMENTS

J.M.C. and J.B. gratefully acknowledge FCT (Fundação para a Ciência e a Tecnologia de Portugal) for the concession of postdoctoral and Ph.D. grants, respectively (contracts: SFRH/BPD/75259/2010 and SFRH/BD/47622/2008). Prof. Maria Pilar Gonçalves (Faculdade de Engenharia da Universidade do Porto) is acknowledged for the kind gift of protein samples.

■ REFERENCES

(1) Nakanishi, K.; Sakiyama, T.; Imamura, K. On the Adsorption of Proteins on Solid Surfaces, a Common but Very Complicated Phenomenon. *J. Biosci. Bioeng.* **2001**, *91*, 233−244.

(2) Rabe, M.; Verdes, D.; Seeger, S. Understanding Protein Adsorption Phenomena at Solid Surfaces. *Adv. Colloid Interface Sci.* **2011**, *162*, 87−106.
(3) Walkey, C. D.; Chan, W. C. Understanding and Controlling the Interaction of Nanomaterials with Proteins in a Physiological Environment. *Chem. Soc. Rev.* **2012**, *41*, 2780−2799.
(4) Palivan, C. G.; Fischer-Onaca, O.; Delcea, M.; Itel, F.; Meier, W. Protein-Polymer Nanoreactors for Medical Applications. *Chem. Soc. Rev.* **2012**, *41*, 2800−2823.
(5) Moyano, D. F.; Rotello, V. M. Nano Meets Biology: Structure and Function at the Nanoparticle Interface. *Langmuir* **2011**, *27*, 10376−10385.
(6) Malmsten, M. Formation of Adsorbed Protein Layers. *J. Colloid Interface Sci.* **1998**, *207*, 186−199.
(7) Koutsoukos, P. G.; Norde, W.; Lyklema, J. Protein Adsorption on Hematite (α-Fe_2O_3) Surfaces. *J. Colloid Interface Sci.* **1983**, *95*, 385−397.
(8) Demanèche, S.; Chapel, J. P.; Monrozier, L. J.; Quiquampoix, H. Dissimilar pH-dependent Adsorption Features of Bovine Serum Albumin and Alpha-Chymotrypsin on Mica Probed by AFM. *Colloids Surf., B* **2009**, *70*, 226−231.
(9) Höök, F.; Rodahl, M.; Kasemo, B.; Brzezinski, P. Structural Changes in Hemoglobin During Adsorption to Solid Surfaces: Effects of pH, Ionic Strength, and Ligand Binding. *Proc. Natl. Acad. Sci. U.S.A.* **1998**, *95*, 12271−12276.
(10) Israelachvili, J. *Intermolecular and Surface Forces*, 2nd ed.; Academic Press: London, 1992.
(11) Kunz, W.; Henle, J.; Ninham, B. W. 'Zur Lehre von der Wirkung der Salze' (About the Science of the Effect of Salts): Franz Hofmeister's Historical Papers. *Curr. Opin. Colloid Interface Sci.* **2004**, *9*, 19−37.
(12) Andrade, J. D.; Hlady, V. Protein Adsorption and Materials Biocompatibility: A Tutorial Review and Suggested Hypotheses. *Adv. Polym. Sci.* **1986**, *79*, 1−63.
(13) Han, M.; Sethuraman, A.; Kane, R. S.; Belfort, G. Nanometer-Scale Roughness has Little Effect on the Amount or Structural Stability of Adsorbed Protein. *Langmuir* **2003**, *19*, 9868−9872.
(14) Frank, B. P.; Belfort, G. Atomic Force Microscopy for Low-Adhesion Surfaces: Thermodynamic Criteria, Critical Surface Tension, and Intermolecular Forces. *Langmuir* **2001**, *17*, 1905−1912.
(15) Anand, G.; Sharma, S.; Dutta, A. K.; Kumar, S. K.; Belfort, G. Conformational Transitions of Adsorbed Proteins on Surfaces of Varying Polarity. *Langmuir* **2010**, *26*, 10803−10811.
(16) Johnson, C. A.; Wu, P.; Lenhoff, A. M. Electrostatic and van der Waals Contributions to Protein Adsorption: 2. Modeling of Ordered Arrays. *Langmuir* **1994**, *10*, 3705−3713.
(17) Roth, C. M.; Lenhoff, A. M. Electrostatic and van der Waals Contributions to Protein Adsorption: Comparison of Theory and Experiment. *Langmuir* **1995**, *11*, 3500−3509.
(18) Sousa, A.; Sengonul, M.; Latour, R.; Kohn, J.; Libera, M. Selective Protein Adsorption on a Phase-Separated Solvent-Cast Polymer Blend. *Langmuir* **2006**, *22*, 6286−6292.
(19) Wang, Y.; Du, X. Miscibility of Binary Monolayers at the Air-Water Interface and Interaction of Protein with Immobilized Monolayers by Surface Plasmon Resonance Technique. *Langmuir* **2006**, *22*, 6195−6202.
(20) Uto, K.; Yamamoto, K.; Kishimoto, N.; Muraoka, M.; Aoyagi, T.; Yamashita, I. Electrostatic Adsorption of Ferritin, Proteins and Nanoparticle Conjugate onto the Surface of Polyelectrolyte Multilayers. *Phys. Chem. Chem. Phys.* **2008**, *18*, 3876−3884.
(21) Campiña, J. M.; Souza, H. K. S.; Borges, J.; Martins, A.; Gonçalves, M. P.; Silva, F. Studies on the Interactions between Bovine β-lactoglobulin and Chitosan at the Solid−Liquid Interface. *Electrochim. Acta* **2010**, *55*, 8779−8790.
(22) Hartvig, R. A.; van de Weert, M.; Østergaard, J.; Jorgensen, L.; Jensen, H. Protein Adsorption at Charged Surfaces: The Role of Electrostatic Interactions and Interfacial Charge Regulation. *Langmuir* **2011**, *27*, 2634−2643.
(23) Elter, P.; Lange, R.; Beck, U. Electrostatic and Dispersion Interactions during Protein Adsorption on Topographic Nanostructures. *Langmuir* **2011**, *27*, 8767−8775.
(24) Hashimoto, T.; Gamo, K.; Fukuta, M.; Zheng, B.; Zettsu, N.; Yamashita, I.; Uraoka, Y.; Watanabe, H. Control of Selective Adsorption Behavior of Ti-binding Ferritin on a SiO2 Substrate by Atomic-Scale Modulation of Local Surface Charges. *Appl. Phys. Lett.* **2011**, *99*, 263701(1)−263701(4).
(25) Borges, J.; Campiña, J. M.; Silva, A. F. Chitosan Biopolymer−F(ab́)$_2$ Immunoconjugate Films for Enhanced Antigen Recognition. *J. Mater. Chem. B* **2013**, *1*, 500−511.
(26) Satriano, C.; Svedhem, S.; Kasemo, B. Well-Defined Lipid Interfaces for Protein Adsorption Studies. *Phys. Chem. Chem. Phys.* **2012**, *14*, 16695−16698.
(27) Prime, K. L.; Whitesides, G. M. Self-Assembled Organic Monolayers: Model Systems for Studying Adsorption of Proteins at Surfaces. *Science* **1991**, *252*, 1164−1167.
(28) Ulman, A. Formation and Structure of Self-Assembled Monolayers. *Chem. Rev.* **1996**, *96*, 1533−1554.
(29) Ostuni, E.; Yan, L.; Whitesides, G. M. The Interaction of Proteins and Cells with Self-Assembled Monolayers of Alkanethiolates on Gold and Silver. *Colloids Surf., B* **1999**, *15*, 3−30.
(30) Bartlett, P. N.; Cooper, J. M. A Review of the Immobilization of Enzymes in Electropolymerized Films. *J. Electroanal. Chem.* **1993**, *362*, 1−12.
(31) Borges, J.; Campiña, J. M.; Souza, H. K. S.; Gonçalves, M. P.; Silva, A. F. Aggregation-Induced Conformational Transitions in Bovine β-Lactoglobulin Adsorbed onto Open Chitosan Structures. *Soft Matter* **2012**, *8*, 1190−1201.
(32) Verity, J. E.; Chhabra, N.; Sinnathamby, K.; Yip, C. M. Tracking Molecular Interactions in Membranes by Simultaneous ATR-FTIR-AFM. *Biophys. J.* **2009**, *97*, 1225−1231.
(33) Glasmästar, K.; Larsson, C.; Höök, F.; Kasemo, B. Protein Adsorption on Supported Phospholipid Bilayers. *J. Colloid Interface Sci.* **2002**, *246*, 40−47.
(34) Khelasvili, G.; Weinstein, H.; Harries, D. Protein Diffusion on Charged Membranes: A Dynamic Mean-Field Model Describes Time Evolution and Lipid Reorganization. *Biophys. J.* **2008**, *94*, 2580−2597.
(35) Zhdanov, V. P.; Kasemo, B. Protein Adsorption and Desorption on Lipid Bilayers. *Biophys. Chem.* **2010**, *146*, 60−64.
(36) Rizzuti, B.; De Santo, M. P.; Guzzi, R. Native β-Lactoglobulin Self-Assembles into a Hexagonal Columnar Phase on a Solid Surface. *Langmuir* **2010**, *26*, 1090−1095.
(37) Whitnah, C. H. The Surface Tension of Milk. A Review. *J. Dairy Sci.* **1959**, *42*, 1437−1449.
(38) Norde, W. Driving Forces for Protein Adsorption at Solid Surfaces. In *Biopolymers at Interfaces*; Malmsten, M., Ed.; CRC Press: New York, 2003; Vol. *110*, pp 21−44.
(39) Norde, W. My Voyage of Discovery to Proteins in Flatland...and Beyond. *Colloids Surf., B* **2008**, *61*, 1−9.
(40) Janshoff, A.; Galla, H. J.; Steinem, C. Piezoelectric Mass-Sensing Devices as Biosensors-An Alternative to Optical Biosensors? *Angew. Chem., Int. Ed.* **2000**, *39*, 4004−4032.
(41) Rodahl, M.; Höök, F.; Fredriksson, C.; Keller, C. A.; Krozer, A.; Brzezinski, P.; Voinova, M.; Kasemo, B. Simultaneous Frequency and Dissipation Factor QCM Measurements of Biomolecular Adsorption and Cell Adhesion. *Faraday Discuss.* **1997**, *107*, 229−246.
(42) Zhao, J.; Luo, L.; Yang, X.; Wang, E.; Dong, S. Determination of Surface pKa of SAM Using an Electrochemical Titration Method. *Electroanalysis* **1999**, *11*, 1108−1111.
(43) Smalley, J. F.; Chalfant, K.; Feldberg, S. W.; Nahir, T. M.; Bowden, E. F. An Indirect Laser-Induced Temperature Jump Determination of the Surface pKa of 11-Mercaptoundecanoic Acid Monolayers Self-Assembled on Gold. *J. Phys. Chem. B* **1999**, *103*, 1676−1685.
(44) Degefa, T. H.; Schön, P.; Bongard, D.; Walder, L. Elucidation of the Electron Transfer Mechanism of Marker Ions at SAMs with Charged Head Groups. *J. Electroanal. Chem.* **2004**, *574*, 49−62.

(45) Hambling, S. G.; McAlpine, A. S.; Sawyer, L. β-lactoglobulin. In *Advanced Dairy Chemistry*; Fox, P., Ed.; Elsevier Applied Science Publishers Ltd.: London, 1992; Vol. *1*, pp 141−190.
(46) Campiña, J. M.; Martins, A.; Silva, F. Selective Permeation of a Liquidlike Self-Assembled Monolayer of 11-Amino-1-undecanethiol on Polycrystalline Gold by Highly Charged Electroactive Probes. *J. Phys. Chem. C* **2007**, *111*, 5351−5362.
(47) Han, J.; Zhang, J.; Xia, Y.; Li, S.; Jiang, L. An Immunoassay in which Magnetic Beads Act both as Collectors and Sensitive Amplifiers for Detecting Antigens in a Microfluidic Chip (MFC)-Quartz Crystal Microbalance (QCM) System. *Colloids Surf., A* **2011**, *379*, 2−9.
(48) Pandey, L. M.; Pattanayek, S. K. Hybrid Surface from Self-Assembled Layer and its Effect on Protein Adsorption. *Appl. Surf. Sci.* **2011**, *257*, 4731−4737.
(49) Köstler, S.; Delgado, A. V.; Ribitsch, V. Surface Thermodynamic Properties of Polyelectrolyte Multilayers. *J. Colloid Interface Sci.* **2005**, *286*, 339−348.
(50) Zhao, Z.-X.; Wang, H.-C.; Qin, X.; Wang, X.-S.; Qiao, M.-Q.; Anzai, J.-I.; Chen, Q. Self-Assembled Film of Hydrophobins on Gold Surfaces and its Application to Electrochemical Biosensing. *Colloids Surf., B* **2009**, *71*, 102−106.
(51) Anand, G.; Zhang, F.; Lindhart, R. J.; Belfort, G. Protein-Associated Water and Secondary Structure Effect Removal of Blood Proteins from Metallic Substrates. *Langmuir* **2011**, *27*, 1830−1836.
(52) San Paulo, A.; Garcia, R. High-Resolution Imaging of Antibodies by Tapping-Mode Atomic Force Microscopy: Attractive and Repulsive Tip-Sample Interaction Regimes. *Biophys. J.* **2000**, *78*, 1599−1605.
(53) Verheul, M.; Pedersen, J. S.; Roefs, S. P. F. M.; Kruif, K. G. D. Association Behavior of Native Beta-Lactoglobulin. *Biopolymers* **1999**, *49*, 11−20.
(54) Wiesbauer, J.; Prassl, R.; Nidetzky, B. Renewal of the Air−Water Interface as a Critical System Parameter of Protein Stability: Aggregation of the Human Growth Hormone and Its Prevention by Surface-Active Compounds. *Langmuir*, Article ASAP, DOI: 10.1021/la4028223.
(55) Elofsson, U. M.; Paulsson, M. A.; Arnebrant, T. Adsorption of β-Lactoglobulin A and B in Relation to Self-Association: Effect of Concentration and pH. *Langmuir* **1997**, *13*, 1695−1700.
(56) Glomm, W. R.; Halskau, O., Jr.; Hanneseth, A.-M. D.; Volden, S. Adsorption Behavior of Acidic and Basic Proteins onto Citrate-Coated Au Surfaces Correlated to Their Native Fold, Stability, and pI. *J. Phys. Chem. B* **2007**, *111*, 14329−14345.
(57) Ramsden, J. J. Puzzles and Paradoxes in Protein Adsorption. *Chem. Soc. Rev.* **1995**, *24*, 73−78.
(58) Messina, G. M. L.; Satriano, C.; Marletta, G. A Multitechnique Study of Preferential Protein Adsorption on Hydrophobic and Hydrophilic Plasma-Modified Polymer Surfaces. *Colloids Surf., B* **2009**, *70*, 76−83.
(59) Qin, B. Y.; Bewley, M. C.; Creamer, L. K.; Baker, H. M.; Baker E. N.; Jameson, G. B. Structural Basis of the Tanford Transition of Bovine β-Lactoglobulin. *Biochemistry* **1998**, *37*, 14014−14023; Crystallographic structure and sequence in: http://www.pdb.org/pdb/explore/explore.do?structureId=3BLG.
(60) Reichhart, C.; Czeslik, C. Native-like Structure of Proteins at a Planar Poly(acrylic acid) Brush. *Langmuir* **2009**, *25*, 1047−1053.
(61) Wahlgren, M.; Arnebrant, T. Adsorption of β-Lactoglobulin onto Silica, Methylated Silica, and Polysulfone. *J. Colloid Interface Sci.* **1990**, *136*, 259−265.
(62) Zhou, C.; Friedt, J.-M.; Angelova, A.; Choi, K.-H.; Laureyn, W.; Frederix, F.; Francis, L. A.; Campitelli, A.; Engelborghs, Y.; Borghs, G. Human Immunoglobulin Adsorption Investigated by Means of Quartz Crystal Microbalance Dissipation, Atomic Force Microscopy, Surface Acoustic Wave, and Surface Plasmon Resonance Techniques. *Langmuir* **2004**, *20*, 5870−5878.
(63) Czarnik-Matusewicz, B.; Murayama, K.; Wu, Y.; Ozaki, Y. Two-Dimensional Attenuated Total Reflection/Infrared Correlation Spectroscopy of Adsorption-Induced and Concentration-Dependent Spectral Variations of β-Lactoglobulin in Aqueous Solutions. *J. Phys. Chem. B* **2000**, *104*, 7803−7811.
(64) Zhou, X.; Zhou, J. Protein Microarrays on Hybrid Polymeric Thin Films Prepared by Self-Assembly of Polyelectrolytes for Multiple-Protein Immunoassays. *Proteomics* **2006**, *6*, 1415−1426.
(65) Cheng, Q.; Brajter-Toth, A. Permselectivity, Sensitivity, and Amperometric pH Sensing at Thioctic Acid Monolayer Microelectrodes. *Anal. Chem.* **1996**, *68*, 4180−4185.
(66) Barton, A. C.; Collyer, S. D.; Davis, F.; Garifallou, G. Z.; Tsekenis, G.; Tully, E.; ÓKennedy, R.; Gibson, T.; Millner, P. A.; Higson, S. P. Labeless AC Impedimetric Antibody-based Sensors with pg mL^{-1} Sensitivities for Point-of-care Biomedical Applications. *Biosens. Bioelectron.* **2009**, *24*, 1090−1095.
(67) Silva, T. H.; Garcia-Morales, V.; Moura, C.; Manzanares, J. A.; Silva, F. Electrochemical Impedance Spectroscopy of Polyelectrolyte Multilayer Modified Gold Electrodes: Influence of Supporting Electrolyte and Temperature. *Langmuir* **2005**, *21*, 7461−7467.